Enhanced Electro-hydrodynamics for Electrospinning a Highly Sensitive Flexible Fiber-Based Piezoelectric Sensor

Trung-Hieu Vu,* Hang Thu Nguyen, Jarred W. Fastier-Wooller, Canh-Dung Tran, Tuan-Hung Nguyen, Hong-Quan Nguyen, Thanh Nguyen, Tuan-Khoa Nguyen, Toan Dinh, Tung T. Bui, Yulin Zhong, Hoang-Phuong Phan, Nam-Trung Nguyen, Dzung V. Dao, and Van Thanh Dau*

ABSTRACT: The single-jet mode in an electro-hydrodynamic (EHD) system is the most desirable mode for generating uniform droplets and fibers and has many applications in numerous fields. Several studies have been carried out to enhance the performance of the EHD process focusing on this mode. In this paper, we introduce the use of a chamfered nozzle in an EHD system to greatly extend the single-jet mode's voltage range, and generally, to enhance the EHD process in terms of control capability and product quality. We carried out simulations and experiments to compare the performance of a chamfered nozzle and conventional flat-end nozzle. Both theoretical analysis and experiments demonstrate that the chamfered nozzle in an EHD system reduces the critical voltage, broadens the voltage range for the single-jet mode, and enhances homogeneity in particle and fiber generation. Furthermore, the chamfered nozzle's advantages were demonstrated in fabricating highly uniform polyvinylidene fluoride-co-trifluoroethylene (PVDF-TrFE) fibers for piezoelectric sensor development. Owing to the fibers' excellent quality, the sensor shows high sensitivity that can detect and differentiate between the drops of a metal bead, a water droplet, and an oil droplet. The use of a chamfered nozzle with its advantages shows potential for development of better EHD-based devices.

KEYWORDS: *flexible piezoelectric sensor, single-jet electro-hydrodynamics, PVDF fibers, polymer electrospray, water droplet sensing, PVDF-TrFE sensor, enhanced electro-hydrodynamics*

1. INTRODUCTION

Electrospraying and electrospinning are two versatile electro-hydrodynamic (EHD) techniques for generating nanoparticles and nanofibers using strong electric fields [1−3]. The particles and fibers within this scale have been studied and applied in numerous applications. In drug delivery, electrospray can be tuned to encapsulate smaller particles of substances such as proteins, nucleotides, cells, etc. in particles generated by electro-spraying[4]. Luo et al. [5] have demonstrated the ability to promote chronic wound healing in rats by delivering protein loaded κ-carrageenan micro-particles to the wound surface. Electrospray allows researchers to tailor the micro-particles' size and porosity to control the drug release mechanism. As particles are good for adsorption, Wang *et al*. [6] used calcinated pollen grains dispersed in magnetic nanoparticles to adsorb oil pollutants and low-density lipoproteins. The controllable movement combined with excellent adsorption ability demonstrates the promising potential of such particles. Due to the large surface areas, nanofibers are also highly facile and can be tuned or loaded with other substances to fit specific purposes such as virus capture [7], water capture [8] and drug delivery [9]. Hence, the improvement of EHD techniques is beneficial for the fabrication of nanoparticles and nanofibers. Fundamentally, an EHD system generally forces a solution to flow through a capillary tube while maintaining a high electrical potential to a grounded electrode. The electric field induces an electrostatic pressure on the liquid droplet at the tube's outlet, which equalizes with the capillary pressure, caused by the liquid's surface tension, to yield a cone-like shaped droplet. This droplet is referred to as a Taylor cone [10]. As the electric field becomes stronger, the electrostatic force overcomes the surface tension, forming a jet at the cone's apex before disintegrating and generating particles or fibers. The shape of the liquid meniscus appearing at the end of the nozzle and the associated mechanism of the disintegration of the jet into an aerosol define a spraying mode [10, 11]. The main modes are dripping, single-jet, and multi-jet. The single-jet mode, also known as the cone-jet mode, generally consists of a Taylor cone that ejects a single liquid thread.

This mode is the most controllable, highly applicable, and it can produce particles/fibers with high homogeneity. Researchers have been studying and improving these techniques to apply them in different fields [12].

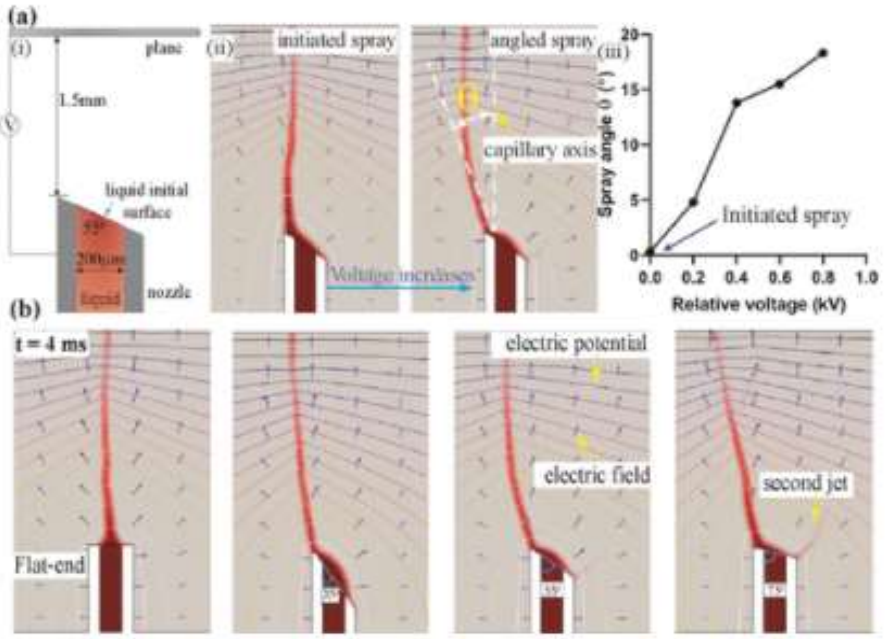

Figure 1. Numerical simulation of the electrospray at the nozzle tip and surrounding for the two nozzles. (a) Simulation of a 55° chamfered nozzle (i) simulation setup, (ii) initial jet from the sharp tip and angle θ as the applied voltage increases, and (iii) spray angle θ plotted vs the applied voltage; and (b) transient simulation of the jet formation for normal flat tip and chamfered sharp tip nozzles (at *t* = 4 ms) with different chamfered angles (35, 55, and 75°): liquid meniscus movement by red color, potential distribution (contour lines), and electric field direction (blue arrows).

Mass spectrometry is the field where electrospray is widely applied. Many studies have been carried out to experiment with various spraying electrode substrates. For example, a solid needle or wire [13], or a gold-coated glass rod [14] was used as a spraying electrode in place of a capillary needle. Non-capillary electrodes have the advantage of an uncomplicated fabrication process and disposability. Another approach is to use non-metal electrodes such as (i) paper, used as a medium for sample loading and ionization, and this has been achieved by applying a high voltage on a piece of paper [15,16], (ii) a wooden tip was utilized for loading and ionizing by dipping the tip into sample solution [17]. The hydrophilic and porous properties of wood and paper allows for effective adhesion of the sample solution to the surface, leading to the successful delivery of particles. Other effective materials for the electrode substrate include leaves [18], acupuncture needles [19], conductive polymer substrates [20] hollow porous fibers [21] or plastic tubes [22]. Even though these studies improved the use of EHD in various applications, they showed limitations in controlling the stability of the spraying mode. Approaches using nozzles with modified geometry have shown to be able to improve this stability of EHD techniques [23].

The use of a flat-end nozzle in a conventional electrospray system has disadvantages regarding jet controllability. In a system with a flat-end nozzle, due to the geometry of the nozzle tip, the liquid droplet is sensitive to disturbances and can form an apex at unintentional positions under an elevated voltage. Thus, jets tend to deviate from the injection axis. This critically influences the spraying stability and dimensions of final products. As such, several solutions have been proposed to address these issues. Morad *et al.* [24] installed a hemispherical cap above the nozzle tip to generate a more stable cone-jet. Their nozzle produced a much broader range of flow rates for the single-jet mode, yielding a

significant increase in practical uses [25]. A more common method to stabilize the flow continuity of the substrate is performed by inserting a thin wire electrode into the capillary tube [26], Ueda *et al*. [27] found that a metal nozzle with multiple tips enhanced the multi-jet mode's spray stability for coating purposes. Similarly, several gas-assisted electro-hydrodynamic atomization (EHDA) systems utilize an external airflow that either moves up to 100 m/s surrounding the liquid core [28−30] or drags the liquid along the low-pressure region induced by high airflow to stabilize the cone jet [31, 32]. These approaches focus on controlling an EHD system by refining, modifying, and improving principal parameters.

In general, these techniques aim to increase single-jet mode stability as well as uniformity of products fabricated by the EHD processes. In this work, the geometrical shape of the electrode tip in EHD was studied. A flat-end nozzle was compared with a chamfered nozzle via simulations and experiments. The comparison indicates that the proposed EHD system with the chamfered nozzle is superior to the conventional EHD system, which uses a flat-end nozzle. The use of the chamfered nozzle in the EHD process has improved stability, reduced clogging, decreased droplet/fiber size, and improved homogeneity.

Furthermore, we applied this enhanced EHD system to fabricate a fiber-based piezoelectric sensor. The sensor exhibited a good piezoelectric sensing performance, in which it could detect tiny liquid droplets as well as a metal bead dropped from a height of 10 cm.

2. DESIGN AND SIMULATION

The critical voltage for an EHD system can be calculated via the relationship of the droplet pressure at a capillary tip and the normal electrostatic pressure caused by the applied voltage. This is shown as $\gamma/r = \varepsilon E2/2$, where, γ is the surface tension, r is the radius of the output nozzle, E is the normal electric field corresponding to the applied voltage, and ε is the surrounding medium's permittivity [33]. An EHD process with a chamfered nozzle has two advantages: (i) facilitates spraying at a lower critical voltage, i.e., the minimum voltage value required to eject a jet from a Taylor cone is lower, and (ii) ability to direct the spraying jet to create an angle θ to the capillary axis. When a liquid is extruded from the capillary, it migrates to the chamfered nozzle's tip due to the Coanda effect [34]. Owing to the sharp tip, the voltage creates a stronger electric field and a larger effective meniscus radius r, i.e., a lower capillary pressure, in comparison with the EHD system using the flat-end nozzle [35]. These factors facilitate the jet from the Taylor cone's apex as the electrostatic force increases. Therefore, a relevant chamfered angle for the nozzle plays a vital role in initially directing the spraying and reducing the critical voltage required to initiate the spraying process.

The generation of the spray jet can be simulated using a computational fluid dynamic model.36 The simulation was carried out using COMSOL Multi-physics software (COMSOL Inc). The simulated liquid is isopropyl alcohol whose properties are σ_s = 20.8 mN/m, μ_{liquid} = 0.0016 Pas, ρ_{liquid} = 0.78 g/mL, and ε_{liquid} = 18. The capillary electrodes are chamfered with different angles of 35, 55, and 75°. The ground electrode is set up perpendicular to the capillary electrode at 1.5 mm from the chamfered tip. The model of simulation and boundary conditions are presented in the Supporting Information, Section 11.

The spray direction using a chamfered angle of 55° is shown in Figure 1a. Due to the concentrated electric field, the liquid forms an apex at the sharp tip of the chamfered nozzle, which ejects the jet of the electrospray at a lower critical voltage. As the applied voltage increases, the spray jet tends to skew away from the electrode axis, which creates an angle θ, as shown in Figure 1a(ii). The relationship between the spraying direction and the applied voltage by experimental observation is given in Figure

1a(iii). This single-jet mode of spray indicates that the jet creates an angle that increases with voltage before transitioning to other modes.

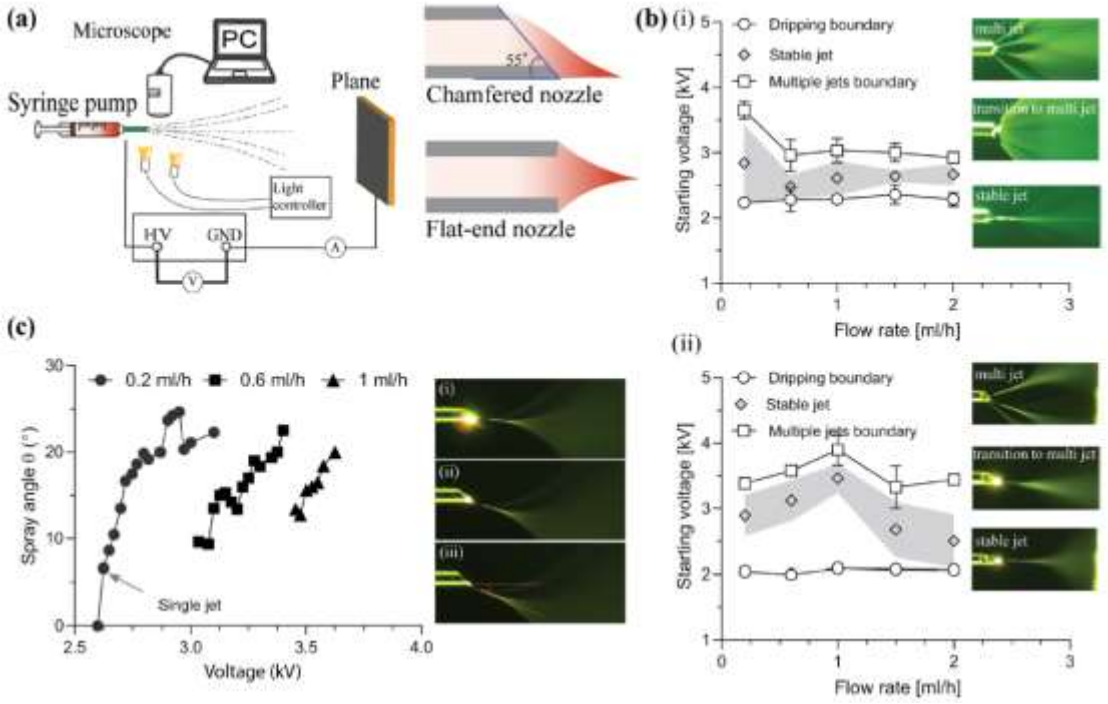

Figure 2. Experiment of the present bipolar electrospray with two types of nozzles (chamfered and flat-end). (a) Experimental setup. (b) Spraying modes' characteristics: (i) applied voltage vs flow rate for the electrospray using a flat-end nozzle and (ii) 55° chamfered nozzle. Insets in panel (b) display the spraying modes. (c) Spraying angle plotted against the applied voltage for three flow rates: 0.2, 0.6, and 1 mL/h. The insets in panel (c) show the transition of the spray angle from (i) low voltage with a small angle to (iii) high voltage with a large angle

3. EXPERIMENTAL RESULTS AND DISCUSSION

The experiment is described in Figure 2a and in more detail in our recent work [37, 38]. We use two types of nozzles with the same inner diameter (Mushashi Engineering), one is a flat-end and the other is chamfered at 55°. Prior to supplementary experiments, we have found that 35 and 75° chamfered nozzles are not as suitable to control as the 55° one. The greater cut area and sharp tip of the 35° nozzle make it more susceptible to solvent evaporation and corona discharge. Similarly, the 75° is more difficult to control stable spray (pictures of the spraying behavior of these nozzles are in the Supporting Information, Section 3 and Figure S3). Thus, the selection of two nozzles, one is chamfered at 55° and the other is 90° (flat-end) nozzles was determined. The working liquid, isopropyl alcohol (Sigma-Aldrich 99.5%), is pumped at a flow rate of 0.2−2 m/h to study the spraying modes of the present system. Other parameters of the experiment are included in the Supporting Information, Section 33.

To compare the results of simulations and morphological photos of the experiment's spraying behaviour, Figure S2 is used to indicate the similarity between the simulation and experiment. From the photo, it can be concluded that the experiment agrees well with the simulation of the 55° chamfered nozzle. The spraying starts at the protruded tip of the nozzle due to the concentrated electric field and the chamfered surface of the nozzle's tip. Experimentally, this results in a tilted Taylor cone as seen in the experimental picture in contrast to a symmetrical Taylor cone seen in conventional electro-spraying with the flat-end nozzle. This tilted spray is consistent with our simulation in the previous section.

3.1. Spray Mode and the Starting Voltage.

We observed three spraying modes as the voltage applied was gradually increased for both the flat-end and the 55° chamfered nozzles (Figure 2b). The modes include the single-jet mode, transitional mode, and multi-jet mode [39]. A dripping mode occurs when the applied voltage is below the critical value and is not discussed due to it not forming strands or droplets. The single-jet mode is defined when a stable electrospray is established with a visible Taylor cone that is then prolonged into a single jet, as observed in the bottom insets (Figure 2b). As the applied voltage continued increasing, the corresponding electric field force overcomes the surface tension of the cone jet, yielding an unstable aerosol dispersion, resulting in a transitional mode. When the voltage reaches the threshold value, the spray enters the multi-jet mode in which the spray jet diverges into multiple distinct jets [10, 40, 41]. While both nozzles experience three spraying modes, the correlation between the applied voltage and flow rate differs for each, as shown in Figure 2a. In general, with all tested flow rates, the critical voltages to initiate the single-jet mode for the chamfered nozzle tip (≈2 kV) are up to 15% lower than the corresponding one using the flat-end nozzle tip (≈2.3 kV). Additionally, the voltage range by which the chamfered nozzle system maintains the single-jet mode before transitioning to the multi-jet region is larger than that of the flat-end nozzle counterpart, as shown in Figure 2b.

The experimental results also depict that the adjustment of the flow rate does not impact the initially applied voltage to generate the electrospray, which fits the approximation of $\gamma/r = (\varepsilon_0 E^2)/2$, as mentioned in Section 2. However, as the flow rate increases, the voltage range that maintains the stable single-jet mode decreases. For example, in the flat nozzle system, the voltage range for stable spraying in the single-jet mode is $\Delta V \approx 2$ kV at a flow rate of 0.2 mL/h decreased to 0.5 kV at 2 mL/h. Meanwhile, the voltage range for the transitioning to the multi-jet mode of the chamfered nozzle system is less affected by the increase of flow rate as seen in Figure 2b (ii). In short, the chamfered nozzle allows stable spray in a wider voltage and flow rate ranges in an electrospray system.

It is worth noting that although this improvement is not tremendous as compared with other studies [24], the present system can initiate electrospray at a significantly lower voltage and is simple to manufacture. Unlike the electrospray using a very sharp electrode, such as an acupuncture needle spray,19 the chamfered nozzle system facilitates corona discharge and it can work with either negative or positive electrospray methods (details can be found in the Supporting Information, Section 5) [42]. These advantages show good potential to improve the development and performance of electrospray devices.

3.2. Spray Angle. The experimental results also confirm that the jet is generated along the direction of the inclined cross section due to the Coanda effect (see insets of Figure 2c) for the chamfered nozzle. This observation corresponds to our simulation, as shown in Figure 1b. For a constant flow rate, the spraying angle θ, defined as the angle between the jet and the capillary axis, tends to increase as the applied voltage increases. At a low voltage, the generated jet aligns with the capillary axis, i.e., the horizontal direction (Figure 2c(i)). As the applied voltage increases, the droplet is stretched, yielding an inclined jet (Figure 2c(ii, iii)). The droplet skews at the nozzle's tip as the voltage increases instead of breaking into multiple jets. This helps the spray remain in the single-jet mode over a wide voltage range.

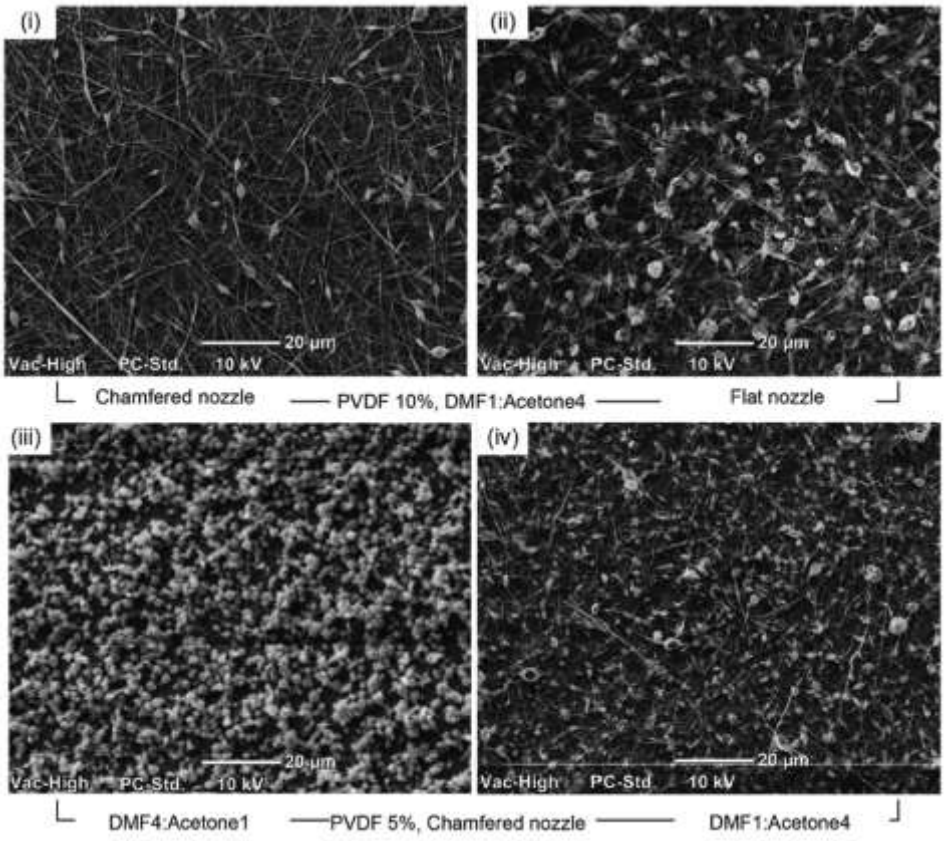

Figure 3. SEM images of polymer beads/fiber fabrication: fiber generation from (i) 55° chamfered nozzle and (ii) flat-end nozzle; particles and beaded fibers generated from the 55° chamfered nozzle with (iii) solution with a low evaporation rate and (iv) solution with a high evaporation rate.

Experimental results also reveal that a higher flow rate requires a greater voltage to keep the jet straight with the visible Taylor cone as demonstrated with the three flow rates: 0.2, 0.6, and 1 mL/h (Figure 2c). While not playing a significant role for the long-distance electrospray, the spray angle can be an effective way to direct and aim aerosols to a near distance target, such as coating spray [43] or jet printing [35].

The spray angles observed in the experiment experience the same trend as the ones predicted from the simulation. Figure 1(iii) suggests that a chamfered nozzle would have a linear relationship between the relative voltage and spray angle in the simulation. The same relationship can be seen in experimental results in Figure 2c. This relationship between the spray angle and applied voltage is consistent across experimented flow rates. This shows that the 55° chamfered angle of the nozzle is approximately optimal for spraying as simulated.

4. GENERATION OF MICRO/NANOFIBERS AND DEVELOPMENT OF A PIEZOELECTRIC SENSOR

4.1. Impact of a Chamfered Nozzle on the Generated Micro/Nanofibers.

Solution blockage is a concern on controlling the EHD system of polymeric solutions with a nozzle that is too large or too small [44]. When the used solvent has a high evaporation rate the solution at the nozzle tip dries quickly, eventually blocking the nozzle, and halting the spraying process [45]. This phenomenon is more noticeable when using smaller nozzles (≈29 Ga nozzle) and impacts the spraying performance negatively. Several approaches were developed to solve this problem, such as (i) using a dual nozzle geometry pumping gas jacket to prevent the quick evaporation of the solvent or (ii) carrying out the experiment at lower temperatures [46]. Using a larger nozzle can prevent this blockage but it requires a higher solution flow rate and applied voltage to produce uniform particles

and fibers [47]. A chamfered nozzle provides a simple solution to this problem. As the electric field plays an important role in the evaporation process [48], the electric field distribution in a chamfered nozzle helps to mitigate the clogging behavior. For a flat-end nozzle, the electric field distributes equally, leading to the evaporation of the solution at the nozzle's outlet and causing clogging in smaller nozzles.

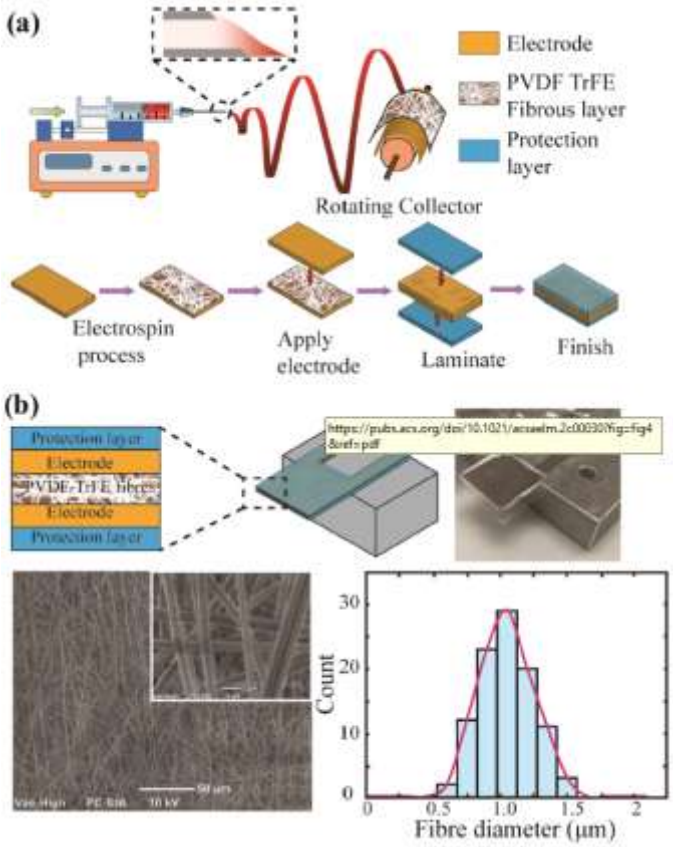

Figure 4. Fabrication of a PVDF-TrFE fibrous mat using the electric field-enhanced electrospinning. (a) Schematic of manufacturing the PVDF-TrFE fibrous mat using the present chamfered nozzle electrospinning and (b) structure of the PVDF-TrFE used sensor and the nanofiber diameter distribution of the electrospun PVDF-TrFE layer.

In contrast, as the electric field is concentrated at the tip of a chamfered nozzle, the solution is under an unequal electric field distribution, leading to a non-uniform evaporation rate at the nozzle's outlet. Hence, the chamfered nozzle is less susceptible to clogging and can be used with highly viscous solutions. In other words, a chamfered nozzle provides the same advantages as using a larger nozzle without the need of applying a higher flow rate or voltage while the inner nozzle diameter is small (≈29 Ga nozzle). Using a small nozzle has the advantage of reducing the voltage and flow rate for uniform particle and fiber fabrication. Thus, this noteworthy finding extends the use of the EHD system in practical applications. For demonstration, solutions of polyvinylidene fluoride (PVDF, M_w= 534 000 g/mol) dissolved in dimethylformamide (DMF): acetone (ACE) with two ratios 1:4 (w/w) and 4:1 (w/w), referred to as solution A and solution B, respectively. Since the vapor pressure of DMF is lower (≈360 Pa) than that of acetone (≈2.4 kPa), the evaporability of the solvent DMF:ACE (4:1) is not as great as the solvent DMF:ACE (1:4). The configuration of the experiment is similar to the setup in Figure 2a with a static grounded plane as the collector. This is designed to compare the two nozzles with regard to the generation of fibers and to demonstrate the advantages of a chamfered nozzle in an EHD system. The two solutions were used with the present system for the experiment with a flow rate of 0.3 mL/h, inter-electrode distance (the distance from the nozzle to the grounded electrode) of

12 cm, and a spraying time of 10 min. The distance of 12 cm ensures that the solvent can evaporate completely and only particles are collected for further analysis. The voltage of ∼12.2 kV was found to be optimal to sustain stable spray at this distance.

The results have shown by electro-hydrodynamics that the morphology of the products can be controlled without blockage (nozzle size ≈29 Ga) using the present chamfered nozzle system. The chamfered nozzle generates fewer polymeric particles/beads and more micro/nanofibers than the flat-end nozzle system at the same voltage (Figure 3(i, ii)). This observation agrees with the discussion mentioned above, as the chamfered nozzle generates a stronger electric field, which facilitates the formation of uniform fibers. For solution A, the chamfered nozzle generates smaller polymeric beads compared to solution B as seen in the SEM images of polymer particles/beads collected on the collector plane/electrode in Figure 3(iii, iv). As predicted, instead of beads, fibers are formed as the polymer concentration increases. This is confirmed by electrospinning PVDF solution with a concentration of 20%. The nanofibers are smooth and free of beads, as shown in the Supporting Information (Figure S6). These results indicate that the chamfered nozzle can enhance the final product of EHD compared to that of the flat-end nozzle.

Furthermore, the chamfered nozzle is capable of producing fibers from polymeric solution (PVDF) at a low concentration of 5%, which can be beneficial for conventional spraying techniques used in previous studies [49, 50]. It is worth noting that the effect of the chamfered nozzle improves the overall electro-hydrodynamic technique without major changes to the solution formulation or experimental setup. This indicates the promising potential to the current fabrication of not only particles but also fibers via electro-hydrodynamics.

4.2. Fabrication and Experiment of a Piezoelectric Sensor via Electric Field-Enhanced Electrospinning.

We further demonstrate how our system can fabricate a functional piezoelectric material by evaluating a piezoelectric sensor with poly (vinylidene fluoride-co-trifluoroethylene) (P(VDF-TrFE)) fibers as the core-sensing element. P(VDF-TrFE), as a copolymer of PVDF, possesses high piezoelectric properties via electrospinning while being ideal for the flexible sensor.

Piezoelectric materials can transform mechanical deformation into electric energy and attract a lot of attention for decades [51−53]. Owing to its flexibility, toughness, and easy processability, (PVDF-TrFE), well known for its piezoelectric properties, shows great potential for piezoelectric sensors [54]. In addition, PVDF-TrFE fibers fabricated from electrospinning were reported to have better piezoelectric properties [55]. Most fiber-based sensor studies overlooked the role of nozzle geometry in the electrospinning process. Thus, in this report, we demonstrate the use of electric field-enhanced electrospinning to fabricate PVDF fibers with a high level of homogeneity for a highly sensitive piezoelectric sensor.

PVDF-TrFE was dissolved in DMF:ACE (3:7) at 20% (w/w). PVDF-TrFE nanofibers were electro-spun with electric field-enhanced electrospinning in a point-drum configuration, as shown in Figure 4a (top). The rotating drum configuration is used as it has the advantage of producing a fibrous mat in a large area [56]. A drum collector was placed 15 cm from the nozzle and acts as a ground electrode. The parameters including an applied voltage of 15 kV, a rotating speed of 1300 rpm, and a flow rate of 1.5 mL/h were found to be optimal to fabricate consistent fibers. The electrospun fibrous mat was collected and examined under a scanning electron microscope (SEM). The average diameter of fibers is 0.97 µm with a standard deviation of only 0.19 µm (Figure 4b, bottom), which demonstrates an improvement in terms of diameter homogeneity over other electrospun fibers [57−59]. The graph's details are indicated in the Supporting Information, Section 7. From previous sections, we hypothesize

that the enhanced electric field and stability from a chamfered nozzle tip is the main reason for dimension consistency. This homogeneity, together with a strong electric field that effectively polarizes the polymer, affects the overall performance of the sensor [60−62].

The XRD analysis (Supporting Information, Section 8) also indicates an improvement over the β-phase formation in both samples generated from the two nozzles in the fiber's structure, which is usually associated with a better piezoelectric response [52, 63]. A comparison between generated fibers from the two nozzles (flat-end and 55° chamfered) indicates a minor difference regarding the [α(100)]/[β(110)/(200)] ratio even though they both show a significant improvement of the βphase formation over precursor powder (Supporting Information, Section 8). Experimental data demonstrate that the use of the chamfered nozzle can produce uniform fibers at a moderately applied voltage (≈15 kV) owing to its enhanced electric field.

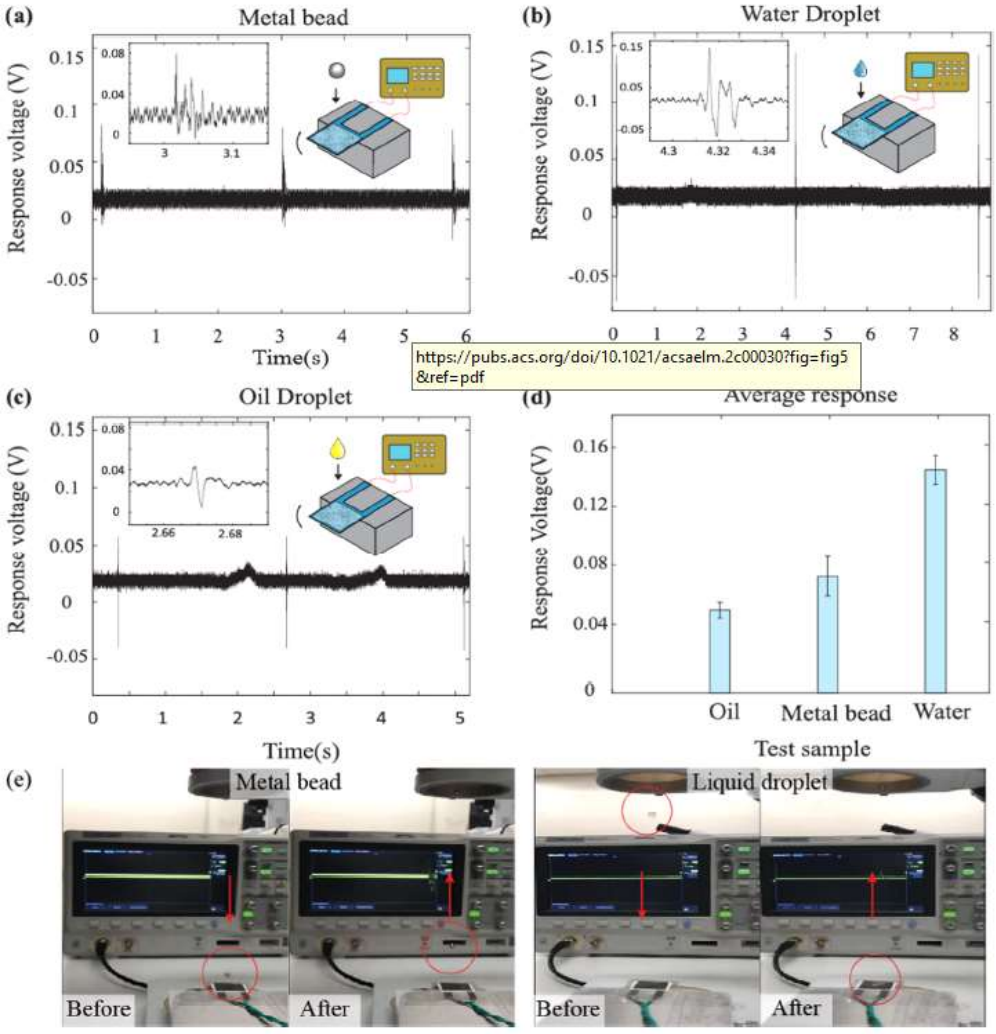

Figure 5. Experimental results showing the time-resolved voltage from a piezoelectric sensor upon being impacted by (a) a metal bead (250 mg), (b) water droplet (70 mg), and (c) oil droplet (40 mg) dropped from a 20 cm height and (d) average output voltage of test samples dropped from a 20 cm height and (e) bounce of a metal bead and how a liquid droplet adheres to the sensor's surface after the impact

The collected PVDF-TrFE fibrous layer is sandwiched between two layers of conductive fabric tape (86750 Nickel/Copper, Laird), which works as the sensor's electrodes. Finally, the sensor was laminated with a polyester film for protection. The sensing area is a square of 25 × 25 mm^2 with an overall thickness of 700 µm (Figure 4b, top right).

The sensor was tested by dropping small metal beads and liquid droplets on its surface from a height of 10, 15, and 20 cm, respectively. After the impact, the sensor deflects and returns to the original position (Figure S9c (ii, iii)). This movement induces a voltage pulse based on the piezoelectric effect, which was monitored with an oscilloscope (DSOX2012A, Keysight Technologies). The weights of metal beads, water droplets, and oil droplets are 250, 70, and 40 mg, respectively. Liquid droplets were dispensed from a nozzle via a system of a syringe pump and tubing at constant flow rates to ensure uniformity (Figure S9a). The output signal is amplified with a gain of 10 before being recorded with the oscilloscope.

Figure 5 shows the voltage response from each impact test of objects dropped from a 20 cm height. The voltage pulse, generated as the sensor deflects, correlates with each object's impact and is distinguishable based on both the pulse magnitude and pulse form. There are two main factors to this response. The first factor is the impact force caused by the object's fall. The shape, weight, and size vary between objects, so the impact force causes distinguishable peak magnitude for each object. In Figure 5a−c, the peaks are consistently distinct from test objects and the average signal in Figure 5d clearly shows an average voltage response. The second factor is the observable behavior of each object as it hits the sensor. A single metal bead hits and bounces off the sensor's surface at the moment of impact and causes vibrations in the sensor (Figure 5e). Figure 5e also presents how a liquid droplet adheres to the sensor after dropping. For a liquid droplet, at the instance of impact, the droplet undergoes multiple stages, leading to changes in droplet shapes and output signals [64]. In our experiment, as the water droplet hits the sensor, it rebounds and its vibration causes the sensor to oscillate before reaching equilibrium (static). This behavior is also illustrated in the insets of Figure 6a with (1) an impact from the drop, (2) the rebounding action, and (3) the oscillation of the droplet and can be seen in Video S2. Each stage corresponds to a peak in the signal recording. Videos S2 and S3 depict the difference between the two droplets' impacts. Unlike the water droplet, the viscosity and surface tension cause an oil droplet to spread slowly without oscillation or recoiling before reaching the static stage [65].

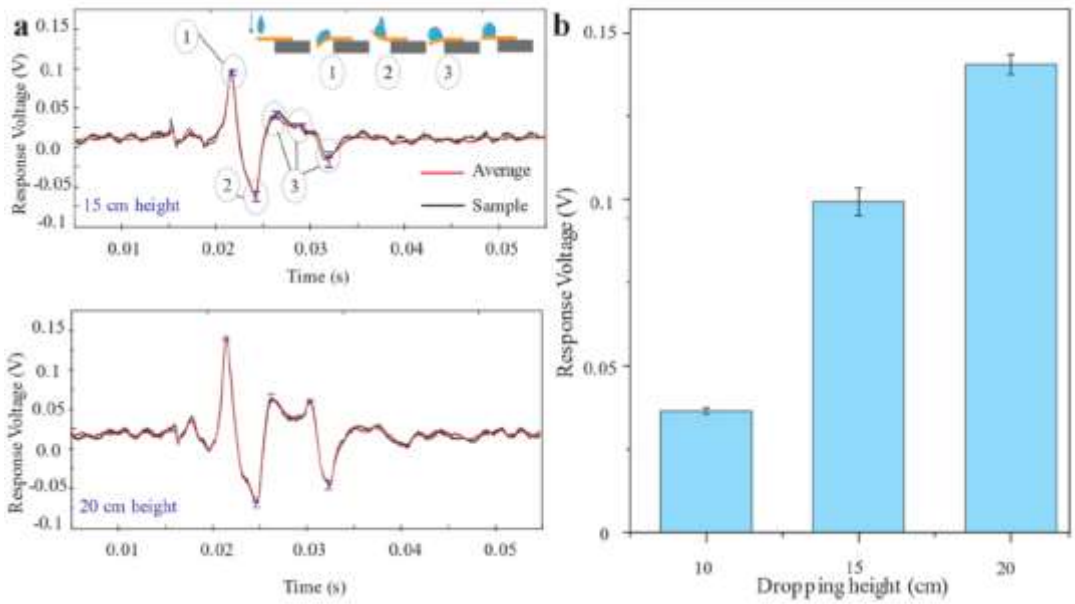

Figure 6. Output behavior under water droplet impact: (a) repeatability test of a water droplet dropped from 15 and 20 cm heights and (b) average response voltage of the water droplet from three different heights: 10, 15, and 20 cm.

In short, the water droplet causes vibrations that can be seen in Figure 5b, inset, while the oil droplet does not. The period needed for the sensor to reach its equilibrium also varies and can be used to detect the object being dropped. The impact by the metal bead lasts the longest (≈100 ms) with seven distinguishable peaks while those by water and oil are ≈50 and ≈20 ms with five and two peaks, respectively (Figure 5a−c insets). As shown in Figure 5d, the average voltage output is 54.5 ± 5.3, 77.5 ± 13, and 149 ± 9.6 mV for the oil droplet, metal bead, and water droplet, respectively. Hence, it can be concluded that by combining all data from the number of peaks, response time, and peak magnitude, the sensor is capable of sensing which object is being dropped. The present sensor can detect as well as differentiate all three test objects despite their insignificant weights, showing an affinity for high sensitivity. Therefore, the sensor with PVDF-TrFE fibers fabricated from our present electrospinning system demonstrated excellent sensing ability for various applications.

The repeatability of water droplet detection over multiple tests is shown in Figure 6. As indicated in the graph (Figure 6a), the output is highly uniform with an average deviation of only ±4.87 mV (or 4.87%) for a 15 cm height and ±3.4 mV (or 2.87%) for a 20 cm height. Thus, it can be concluded that the sensor successfully gives consistent output signals with high repeatability and low deviation in the water droplet impact detection. The greatest peak and its deviation from all heights are presented in Figure 6b. This clearly indicates that the sensor can detect the impact of water droplets.

5. CONCLUSIONS

In this work, we investigated the effect of a chamfered nozzle for EHD processes, including electrospray and electrospinning. The chamfered nozzle at 55° demonstrates the ability to reduce the critical voltage, direct and align jet formation, and produce homogeneous micro/nanoparticles/fibers while being simple to manufacture. The experimental work confirmed that a chamfered nozzle can maintain a wider voltage range for the stable jet, direct aerosols, prevent clogging, and generate homogeneous particles/fibers. These features show potential to improve the performance of EHD devices. We demonstrated this enhanced EHD system to fabricate a PVDF-TrFE piezoelectric sensor with good sensitivity. The proposed sensor was able to detect and distinguish the impacts of a metal bead, water droplet, and oil droplet with different physical properties and negligible weights of 250, 70, and 40 mg, respectively. Findings from this work show that using a chamfered nozzle is a simple method to improve the performance of an electrospray/electrospinning system as well as demonstrate potential for developing high-performance EHD-based devices.

■ ASSOCIATED CONTENT

*Supporting Information

The Supporting Information is available free of charge at https://pubs.acs.org/doi/10.1021/acsaelm.2c00030.

Simulation model; experiment versus simulation of the chamfered nozzle; experimental setup; I−V characteristics; pictures of the spray mode in negative and positive electrosprays; nanofiber generation; polymer solution for piezoelectric fibers; XRD analysis; and the experimental setup for the piezoelectric sensor (PDF)

Video S1 (MP4)

Video S2 (MP4)

Video S3 (MP4)

REFERENCES

[1] Nikolaou, M.; Krasia-christoforou, T. European Journal of Pharmaceutical Sciences Electro-hydrodynamic Methods for the Development of Pulmonary Drug Delivery Systems. Eur. J. Pharm.Sci. 2018, 113, 29−40.

[2] Kavadiya, S.; Biswas, P. Electrospray Deposition of Biomolecules: Applications, Challenges, and Recommendations. J. Aerosol Sci. 2018, 125, 182−207.

[3] Castillo, J. L.; Martin, S.; Rodriguez-Perez, D.; Higuera, F. J.; Garcia-Ybarra, P. L. Nanostructured Porous Coatings via Electrospray Atomization and Deposition of Nanoparticle Suspensions. J. Aerosol Sci. 2018, 125, 148−163.

[4] Steipel, R. T.; Gallovic, M. D.; Batty, C. J.; Bachelder, E. M.; Ainslie, K. M. Electrospray for Generation of Drug Delivery and Vaccine Particles Applied in Vitro and in Vivo. Mater. Sci. Eng. C 2019, 105, No. 110070.

[5] Luo, Z.; Che, J.; Sun, L.; Yang, L.; Zu, Y.; Wang, H.; Zhao, Y. Microfluidic Electrospray Photo-Crosslinkable κ-Carrageenan Microparticles for Wound Healing. Eng. Regener. 2021, 2, 257−262.

[6] Wang, Y.; Sun, L.; Guo, J.; Shi, K.; Shang, L.; Xiao, J.; Zhao, Y. Pollens Derived Magnetic Porous Particles for Adsorption of LowDensity Lipoprotein from Plasma. Bioact. Mater. 2021, 6, 1555−1562.

[7] Merenda, A.; Bortolassi, A. C. C.; Rodriguez-Andres, J.; AlAttabi, R.; Schütz, J. A.; Kujawski, W.; Shon, H. K.; Dumée, L. F. Hybrid Polymer/Ionic Liquid Electrospun Membranes with Tunable Surface Charge for Virus Capture in Aqueous Environments. J. Water Process Eng. 2021, 43, No. 102278.

[8] Yang, C.; Yu, Y.; Wang, X.; Shang, L.; Zhao, Y. Programmable Knot Microfibers from Piezoelectric Microfluidics. Small 2021, 18, No. 2104309.

[9] Eslamian, M.; Khorrami, M.; Yi, N.; Majd, S.; Abidian, M. R. Electrospinning of Highly Aligned Fibers for Drug Delivery Applications. J. Mater. Chem. B 2019, 7, 224−232.

[10] Gañán-Calvo, A. M.; López-Herrera, J. M.; Herrada, M. A.; Ramos, A.; Montanero, J. M. Review on the Physics of Electrospray: From Electrokinetics to the Operating Conditions of Single and Coaxial Taylor Cone-Jets, and AC Electrospray. J. Aerosol Sci. 2018, 125, 32−56.

[11] Hartman, R. P. A.; Brunner, D. J.; Marijnissen, J. C. M.; Scarlett, B. Scaling Laws for Droplet Size and Current Produced in the Cone-Jet Mode. J. Aerosol Sci. 1998, 29, S977−S978.

[12] Jaworek, A.; Ganán-Calvo, A. M.; Machala, Z. Low Temperature Plasmas and Electrosprays. J. Phys. D. Appl. Phys. 2019, 52, No. 233001.

[13] Mandal, M. K.; Chen, L. C.; Hashimoto, Y.; Yu, Z.; Hiraoka, K. Detection of Biomolecules from Solutions with High Concentration of Salts Using Probe Electrospray and Nano-Electrospray Ionization Mass Spectrometry. Anal. Methods 2010, 2, 1905−1912.

[14] Jeng, J.; Shiea, J. Electrospray Ionization from a Droplet Deposited on a Surface-Modified Glass Rod. Rapid Commun. Mass Spectrom. 2003, 17, 1709−1713.

[15] Li, A.; Wang, H.; Ouyang, Z.; Cooks, R. G. Paper Spray Ionization of Polar Analytes Using Non-Polar Solvents. Chem. Commun. 2011, 47, 2811−2813.

[16] Wang, H.; Manicke, N. E.; Yang, Q.; Zheng, L.; Shi, R.; Cooks, R. G.; Ouyang, Z. Direct Analysis of Biological Tissue by Paper Spray Mass Spectrometry. Anal. Chem. 2011, 83, 1197−1201.

[17] Hu, B.; So, P. K.; Chen, H.; Yao, Z. P. Electrospray Ionization Using Wooden Tips. Anal. Chem. 2011, 83, 8201−8207.

[18] Liu, J.; Wang, H.; Cooks, R. G.; Ouyang, Z. Leaf Spray: Direct Chemical Analysis of Plant Material and Living Plants by Mass Spectrometry. Anal. Chem. 2011, 83, 7608−7613.

[19] Wei, Y.; Chen, L.; Zhou, W.; Chingin, K.; Ouyang, Y.; Zhu, T.; Wen, H.; Ding, J.; Xu, J.; Chen, H. Tissue Spray Ionization Mass Spectrometry for Rapid Recognition of Human Lung Squamous Cell Carcinoma. Sci. Rep. 2015, 5, No. 10077.

[20] Song, X.; Chen, H.; Zare, R. N. Conductive Polymer Spray Ionization Mass Spectrometry for Biofluid Analysis. Anal. Chem. 2018, 90, 12878−12885.

[21] Liou, Y. W.; Wang, J. S.; Chen, C. C.; Lin, C. H. Development of an On-Line Microextraction Method for Use in Fiber-Spray/Mass Spectrometry. Int. J. Mass Spectrom. 2017, 421, 178−183.

[22] Huang, Y.-Q.; You, J.-Q.; Yuan, B.-F.; Feng, Y.-Q. Sample Preparation and Direct Electrospray Ionization on a Tip Column for Rapid Mass Spectrometry Analysis of Complex Samples. Analyst 2012, 137, 4593.

[23] Kien Nguyen, T.; Nguyen, V. D.; Seong, B.; Hoang, N.; Park, J.; Byun, D. Control and Improvement of Jet Stability by Monitoring Liquid Meniscus in Electrospray and Electrohydrodynamic Jet. J. Aerosol Sci. 2014, 71, 29−39.

[24] Morad, M. R.; Rajabi, A.; Razavi, M.; Pejman Sereshkeh, S. R. A Very Stable High Throughput Taylor Cone-Jet in Electrohydrodynamics. Sci. Rep. 2016, 6, No. 38509. (25) Rajabi, A.; Javadi, E.; Pejman Sereshkeh, S. R.; Morad, M. R.; Kebriaee, A.; Nasiri, H.; Razavi Haeri, S. A. A. Experimental Characterization of an Extended Electrohydrodynamic Cone-Jet with a Hemispherical Nozzle. Phys. Fluids 2018, 30, No. 114108.

[26] Yogi, O.; Kawakami, T.; Mizuno, A. Properties of Droplet Formation Made by Cone Jet Using a Novel Capillary with an External Electrode. J. Electrostat. 2006, 64, 634−638.

[27] Ueda, H.; Takeuchi, K.; Kikuchi, A. Effect of the Nozzle Tip's Geometrical Shape on Electrospray Deposition of Organic Thin Films. Jpn. J. Appl. Phys. 2017, 56, No. 04CL05.

[28] Sultan, F.; Allaf-Akbari, E.; Ashgriz, N. Effects of a Coflowing Air on the Characteristics of an Electrospray. Aerosol Sci. Eng. 2020, 4, 210−218.

[29] Lee, J. Y.; Kottke, P. A.; Fedorov, A. G. Electrohydrodynamics of Gas-Assisted Electrospray Ionization Mass Spectrometry. J. Am. Soc. Mass Spectrom. 2020, 31, 2073−2085.

[30] Cruz-Mazo, F.; Wiedorn, M. O.; Herrada, M. A.; Bajt, S.; Chapman, H. N.; Gañán-Calvo, A. M. Aerodynamically Stabilized Taylor Cone Jets. Phys. Rev. E 2019, 100, No. 031101.

[31] Zahoor, R.; Bajt, S.; Šarler, B. Influence of Gas Dynamic Virtual Nozzle Geometry on Micro-Jet Characteristics. Int. J. Multiphase Flow 2018, 104, 152−165.

[32] Seong, B.; Hwang, S.; Jang, H. S.; Lee, H.; Kim, J.; Nguyen, V. D.; Cho, D. H.; Lin, L.; Byun, D. A Hybrid Aerodynamic and Electrostatic Atomization System for Enhanced Uniformity of Thin Film. J. Electrostat. 2017, 87, 93−101.

[33] Verdoold, S.; Agostinho, L. L. F.; Yurteri, C. U.; Marijnissen, J. C. M. A Generic Electrospray Classification. J. Aerosol Sci. 2014, 67, 87−103.

[34] Robichaud, G.; Dixon, R. B.; Potturi, A. S.; Cassidy, D.; Edwards, J. R.; Sohn, A.; Dow, T. A.; Muddiman, D. C. Design, Modeling, Fabrication, and Evaluation of the Air Amplifier for Improved Detection of Biomolecules by Electrospray Ionization Mass Spectrometry. Int. J. Mass Spectrom. 2011, 300, 99−107.

[35] Park, J. U.; Hardy, M.; Kang, S. J.; Barton, K.; Adair, K.; Mukhopadhyay, D. K.; Lee, C. Y.; Strano, M. S.; Alleyne, A. G.; Georgiadis, J. G.; Ferreira, P. M.; Rogers, J. A. High-Resolution Electrohydrodynamic Jet Printing. Nat. Mater. 2007, 6, 782−789.

[36] Du, W.; Chaudhuri, S. A Multiphysics Model for Charged Liquid Droplet Breakup in Electric Fields. Int. J. Multiphase Flow 2017, 90, 46−56.

[37] Dau, V. T.; Vu, H. T.; Tran, C.; Nguyen, T. V.; Nguyen, T.-K.; Dinh, T.; Phan, H.; Shimizu, K.; Nguyen, N.; Dao, D. V. Electrospray Propelled by Ionic Wind in a Bipolar System for Direct Delivery of Charge Reduced Nanoparticles. Appl. Phys. Express 2021, 14, No. 055001.

[38] Dau, V. T.; Bui, T. T.; Tran, C. D.; Nguyen, T. V.; Nguyen, T. K.; Dinh, T.; Phan, H. P.; Wibowo, D.; Rehm, B. H. A.; Ta, H. T.; Nguyen, N. T.; Dao, D. V. In-Air Particle Generation by on-Chip Electrohydrodynamics. Lab Chip 2021, 21, 1779−1787.

[39] Ryan, C. N.; Smith, K. L.; Stark, J. P. W. Characterization of Multi-Jet Electrospray Systems. J. Aerosol Sci. 2012, 51, 35−48. (40) Smeets, A.; Clasen, C.; Van den Mooter, G. Electrospraying of Polymer Solutions: Study of Formulation and Process Parameters. Eur. J. Pharm. Biopharm. 2017, 119, 114−124.

[41] Jeong, J.; Choi, H.; Park, K.; Kim, H.; Choi, J.; Park, I.; Lee, S. S. Polymer Micro-Atomizer for Water Electrospray in the Cone Jet Mode. Polymer 2020, 194, No. 122405.

[42] Guo, Y.; Li, S.; Wu, Z.; Zhu, K.; Han, Y.; Wang, N. Interaction between Electrospray Using Ionic Liquid and Simultaneous Corona Discharge under Positive and Negative Polarity. Phys. Plasmas 2019, 26, No. 073511.

[43] Jaworek, A.; Sobczyk, A. T.; Krupa, A. Electrospray Application to Powder Production and Surface Coating. J. Aerosol Sci. 2018, 125, 57−92.

[44] Tripatanasuwan, S.; Zhong, Z.; Reneker, D. Effect of Evaporation and Solidification of the Charged Jet Inelectrospinning of Poly(Ethylene Oxide) Aqueous Solution. Polymer 2007, 48, 5742− 5746.

[45] Zeng, J.; Chen, X.; Xu, X.; Liang, Q.; Bian, X.; Yang, L.; Jing, X. Ultrafine Fibers Electrospun from Biodegradable Polymers. J. Appl. Polym. Sci. 2003, 89, 1085−1092.

[46] Larsen, G.; Spretz, R.; Velarde-Ortiz, R. Use of Coaxial Gas Jackets to Stabilize Taylor Cones of Volatile Solutions and to Induce Particle-to-Fiber Transitions. Adv. Mater. 2004, 16, 166−169.

[47] Youn, D. H.; Kim, S. H.; Yang, Y. S.; Lim, S. C.; Kim, S. J.; Ahn, S. H.; Sim, H. S.; Ryu, S. M.; Shin, D. W.; Yoo, J. B. Electrohydrodynamic Micropatterning of Silver Ink Using NearField Electrohydrodynamic Jet Printing with Tilted-Outlet Nozzle. Appl. Phys. A 2009, 96, 933−938.

[48] Kanjanapongkul, K.; Wongsasulak, S.; Yoovidhya, T. Prediction of Clogging Time during Electrospinning of Zein Solution: Scaling Analysis and Experimental Verification. Chem. Eng. Sci. 2010, 65, 5217−5225.

[49] Costa, L. M. M.; Bretas, R. E. S.; Gregorio, R. Effect of Solution Concentration on the Electrospray/Electrospinning Transition and on the Crystalline Phase of PVDF. Mater. Sci. Appl. 2010, 01, 247−252.

[50] Nasir, M.; Matsumoto, H.; Danno, T.; Minagawa, M.; Irisawa, T.; Shioya, M.; Tanioka, A. Control of Diameter, Morphology, and Structure of PVDF Nanofiber Fabricated by Electrospray Deposition. J. Polym. Sci., Part B: Polym. Phys. 2006, 44, 779−786.

[51] Xin, Y.; Zhu, J.; Sun, H.; Xu, Y.; Liu, T.; Qian, C. A Brief Review on Piezoelectric PVDF Nanofibers Prepared by Electrospinning. Ferroelectrics 2018, 526, 140−151.

[52] Varposhti, A. M.; Yousefzadeh, M.; Kowsari, E.; Latifi, M. Enhancement of β-Phase Crystalline Structure and Piezoelectric Properties of Flexible PVDF/Ionic Liquid Surfactant Composite Nanofibers for Potential Application in Sensing and Self-Powering. Macromol. Mater. Eng. 2020, 305, No. 1900796.

[53] Nguyen, H. Q.; Nguyen, T.; Tanner, P.; Nguyen, T. K.; Foisal, A. R. M.; Fastier-Wooller, J.; Nguyen, T. H.; Phan, H. P.; Nguyen, N. T.; Dao, D. V. Piezotronic Effect in a Normally off P-GaN/AlGaN/ GaN HEMT toward Highly Sensitive Pressure Sensor. Appl. Phys. Lett. 2021, 118, No. 242104.

[54] Jiang, Y.; Gong, L.; Hu, X.; Zhao, Y.; Chen, H.; Feng, L.; Zhang, D. Aligned P(VDF-TrFE) Nanofibers for Enhanced Piezoelectric Directional Strain Sensing. Polymers 2018, 10, No. 364.

[55] Yee, W. A.; Kotaki, M.; Liu, Y.; Lu, X. Morphology, Polymorphism Behavior and Molecular Orientation of Electrospun Poly(Vinylidene Fluoride) Fibers. Polymer 2007, 48, 512−521.

[56] Teo, W. E.; Ramakrishna, S. A Review on Electrospinning Design and Nanofibre Assemblies. Nanotechnology 2006, 17, No. R89.

[57] Szewczyk, P. K.; Gradys, A.; Kim, S. K.; Persano, L.; Marzec, M.; Kryshtal, A.; Busolo, T.; Toncelli, A.; Pisignano, D.; Bernasik, A.; Kar-Narayan, S.; Sajkiewicz, P.; Stachewicz, U. Enhanced Piezoelectricity of Electrospun Polyvinylidene Fluoride Fibers for Energy Harvesting. ACS Appl. Mater. Interfaces 2020, 12, 13575−13583.

[58] Mohseni, M.; Ramazani, S. A. A.; H-Shirazi, F.; Hassanzadeh Nemati, N. Gellan Gel Comprising Short PVDF Based-Nanofibers: The Effect of Piezoelectric Nanofiber on the Mechanical and Electrical Behavior. Mater. Today Commun. 2021, 26, No. 101785.

[59] Hwang, Y. J.; Choi, S.; Kim, H. S. Structural Deformation of PVDF Nanoweb Due to Electrospinning Behavior Affected by Solvent Ratio. E-Polymers 2018, 18, 339−345.

[60] Dinh, T.; Nguyen, T.; Phan, H. P.; Nguyen, T. K.; Dau, V. T.; Nguyen, N. T.; Dao, D. V. Advances in Rational Design and Materials of High-Performance Stretchable Electromechanical Sensors. Small 2020, 16, No. 1905707.

[61] Arrigoni, A.; Brambilla, L.; Bertarelli, C.; Serra, G.; Tommasini, M.; Castiglioni, C. P(VDF-TrFE) Nanofibers: Structure of the Ferroelectric and Paraelectric Phases through IR and Raman Spectroscopies. RSC Adv. 2020, 10, 37779−37796.

[62] Mokhtari, F.; Shamshirsaz, M.; Latifi, M.; Foroughi, J. Nanofibers-Based Piezoelectric Energy Harvester for Self-Powered Wearable Technologies. Polymers 2020, 12, No. 2697.

[63] Chang, C.; Tran, V. H.; Wang, J.; Fuh, Y. K.; Lin, L. DirectWrite Piezoelectric Polymeric Nanogenerator with High Energy Conversion Efficiency. Nano Lett. 2010, 10, 726−731.

[64] Hao, G.; Dong, X.; Li, Z. A Novel Piezoelectric Structure for Harvesting Energy from Water Droplet: Theoretical and Experimental Studies. Energy 2021, 232, No. 121071.

[65] Grinspan, A. S.; Gnanamoorthy, R. Impact Force of Low Velocity Liquid Droplets Measured Using Piezoelectric PVDF Film. Colloids Surf., A 2010, 356, 162−168.